Ảnh hưởng của pha tạp boron đến cấu trúc tinh thể, hình thái, năng lượng vùng cấm và hoạt tính quang xúc tác của g-C_3N_4

TÓM TẮT

g-C_3N_4 và g-C_3N_4 pha tạp boron đã được tổng hợp thành công bằng phương pháp ngưng tụ đơn giản urea và hỗn hợp urea và boric acid tương ứng. Ảnh hưởng của pha tạp boron lên cấu trúc tinh thể, hình thái bề mặt, năng lượng vùng cấm và tính chất quang xúc tác của g-C_3N_4 đã được nghiên cứu một cách có hệ thống thông qua nhiều kỹ thuật khác nhau bao gồm nhiễu xạ tia X (XRD), quang phổ hồng ngoại biến đổi Fourier (FT-IR), hiển vi điện tử quét (SEM) và Quang phổ phản xạ khuếch tán tia cực tím (UV-Vis DRS). Ngoài ra, động học của các phản ứng quang xúc tác và ảnh hưởng của lượng chất xúc tác quang đến hiệu suất phân hủy quang methyl blue (MB) đã được khảo sát. Kết quả cho thấy tất cả các mẫu đều thể hiện hoạt tính quang xúc tác trong vùng ánh sáng khả kiến. Đáng chú ý, mẫu B-g-C_3N_4-1:30-500,550 có hiệu suất phân hủy quang cao nhất, đạt 92%.

Từ khóa: *g-C_3N_4 và g-C_3N_4 pha tạp boron, quang xúc tác, chiếu xạ ánh sáng khả kiến và phân hủy MB.*

Influence of boron doping on the crystal structure, morphology, band gap and photocatalytic activities of g-C_3N_4

ABSTRACT

Undoped g-C_3N_4 and boron-doped g-C_3N_4 photocatalysts were synthesized successfully using the facile condensation method, in which urea and a mixture of urea and boric acid were heated, respectively. The effect of boron-doping on the crystal structure, surface morphology, bandgap energy, and photocatalytic properties of g-C_3N_4 was systematically investigated through various techniques including X-ray diffraction (XRD), Fourier Transform Infrared Spectroscopy (FT-IR), Scanning Electron Microscopy (SEM), and Ultraviolet-Visible Diffuse Reflectance Spectroscopy (UV-Vis DRS). Additionally, the kinetics of photocatalytic reactions and the impact of the photocatalyst amount on the efficiency of Methyl Blue (MB) photodegradation were examined. The results revealed that all samples exhibited photocatalytic activity in the visible light region. Notably, the sample B-g-C_3N_4-1:30-500,550 demonstrated the highest photodegradation efficiency, reaching 92%.

Keywords: *g-C_3N_4, boron-doped g-C_3N_4, photocatalysis, visible-light irradiation, and MB degradation.*

1. INTRODUCTION

Environmental pollution, particularly water pollution caused by persistent organic pollutants, is becoming a major global concern due to the constant growth of population and modern industry.[1] Photocatalysis is considered an attractive method that has gained worldwide attention in research. Photocatalysis, an advanced photochemical oxidation process, has been extensively studied for its potential applications in wastewater treatment. Compared to conventional methods, photocatalysis based on semiconductors offers many advantages**.** In recent years, there has been a notable increase in interest in g-C_3N_4 due to its unique electronic structure,[2,3] suitable bandgap (approximately 2.7 eV) for visible-light-driven photocatalysis,[4] high thermal and chemical stability, and non-toxicity.[5] However, a major drawback of g-C_3N_4 is its fast recombination rate of photo-induced electrons and holes, which reduces its efficiency in degrading organic compounds through photocatalysis.[6] Consequently, the development of g-C_3N_4-based photocatalytic materials with higher activity for wastewater treatment has garnered significant attention from both domestic and foreign.[7,8] Various approaches have been employed to modify the properties of g-C_3N_4, such as metal and non-metal doping,[9] nanostructure modification,[10] and heterojunction construction.[11] Among these approaches, non-metal doping is considered an effective method for lowering the recombination rate of electron-hole pairs and enhancing photocatalytic performance. Recent reports have demonstrated that doping boron into g-C_3N_4 results in unique structural and electronic changes, making it a potential candidate for wastewater treatment.[12,13]

In this paper, we systematically investigate the effect of boron-doping on the crystal structure, surface morphology, bandgap energy, and photocatalytic properties of g-C_3N_4.

2. EXPERIMENT

2.1. Chemicals

All of the starting materials used in this paper were of analytic grade and were ultized without further purification.

2.2. Synthesis of g-C_3N_4 and boron-doped g-C_3N_4

To prepare the mixture of urea and boric acid with different weight ratios, it was necessary to finely grind them together using an agate mortar. Once properly ground, the mixture was transferred into a porcelain bowl and sealed with aluminum foil. This step was crucial to prevent the sublimation of precursors and promote the condensation of products. The sealed bowl containing the mixture was then placed into a

furnace. The annealing process began by heating it at 500 °C for 2 hours. After this initial annealing, the temperature was raised to 550 °C and maintained for another 2 hours. The heating rate during both annealing stages was set at 10 °C per minute. Once the sintering process was finished, the furnace was let to naturally cool down to room temperature before the sample was removed.

To ensure the removal of any unreacted impurities, the obtained sample was washed several times with ethanol. The sample was then denoted as B-g-C_3N_4-n:m, where n:m represents the weight ratio of boric acid to urea (options included 1:10, 1:20, 1:30, 1:40, and 1:80). For comparison purposes, pure g-C_3N_4 was also synthesized following the same procedure, but without the addition of boric acid.

2.3. Material characterizations

Samples were analyzed using X-ray diffraction (XRD) to obtain their XRD patterns. The XRD measurements were conducted at room temperature using a D8 Advance Brucker diffractometer operated at 40 kV and 100 mA, with Cu-Kα radiation ($\lambda_{K\alpha}$ = 1.5406 Å). The scanning range was set between 20 and 80º at a step size of 0.03º. The Fourier Transform Infrared (FT-IR) spectra of the samples were recorded within the range of 4000 to 400 cm^{-1} using an IRAffinity-1S spectrometer. To investigate the optical properties of the photocatalysts, UV-Vis Diffuse Reflectance Spectroscopy (UV-Vis DRS) was performed using a Jasco-V670 UV-Vis spectrometer. The particle size and surface morphology of the samples were examined using Scanning Electron Microscopy (SEM) with a NanoSEM-450 instrument.

2.4. Photocatalytic activities of g-C_3N_4 and B-doped g-C_3N_4

The photocatalytic activities of all the samples obtained were evaluated by studying the degradation of MB in an aqueous solution under visible light irradiation. In this experiment, 0.03 g of the photocatalyst was added to 80 mL of an MB solution with a concentration of 10 mg/L in a 250 mL glass beaker. The mixture was then stirred continuously in the dark for 2 hours, allowing the adsorption and desorption processes of MB molecules on the catalyst surface to reach equilibrium. After this, the synthesized photocatalysts were subjected to six hours of irradiation using a tungsten filament lamp (60 W - 220 V).

At specific intervals of irradiation, 7 mL of the mixed suspension was extracted and centrifuged at 6000 rpm for 20 minutes to remove the catalyst from the mixture. The residual MB concentration was then measured by analyzing the absorbance at 663 nm using a UV-Vis CE-2011 spectrometer. The photodegradation efficiency of MB was calculated using the following formula:

$$H\% = \frac{C_o - C}{C_o}.100$$

In which, C_o is the initial concentration of MB and C is the remaining concentration of MB after each corresponding irradiation time.

3. RESULTS AND CONCLUSION

3.1. Effect of the Boron concentration on the crystal structure of g-C_3N_4

The crystal structure of undoped g-C_3N_4 and boron-doped g-C_3N_4 samples was investigated using XRD and FT-IR techniques. Figure 1 displays the XRD patterns measured at room temperature for both g-C_3N_4 and B-g-C_3N_4-n:m samples.

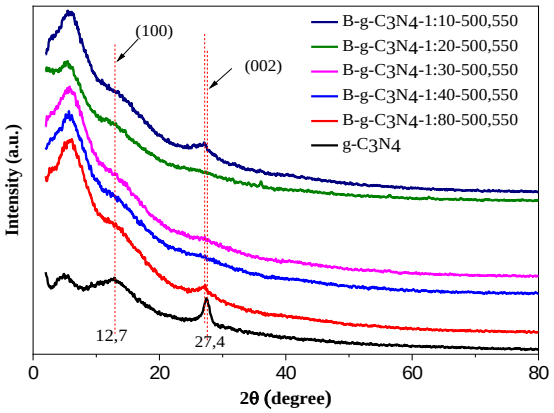

Figure 1. XRD patterns of g-C_3N_4 and B-g-C_3N_4-n:m-500,550.

Experimental results reveal that all samples exhibit two characteristic peaks of g-C_3N_4 at 2θ = 12.7 and 27.4º. This suggests that doping boron into g-C_3N_4 does not alter its crystal structure. The peak at 2θ = 12.7º corresponds to the periodic arrangement of tri-s-triazine units in the crystal plane (100), while the peak at 2θ = 27.4º represents the arrangement of aromatic conjugate systems on the crystal surface (002). Upon introduction of boron, the peak associated with the crystal surface (002) undergoes a slight shift towards smaller angles depending on the concentration of B. This shift may be attributed to the replacement of C or N atoms by B atoms.[14] Furthermore, the intensity of the peak at 2θ = 27.4º decreases with increasing B concentration,

indicating that boron doping results in a decrease in the crystallinity of g-C_3N_4. This finding is consistent with previous reports.[14-16]

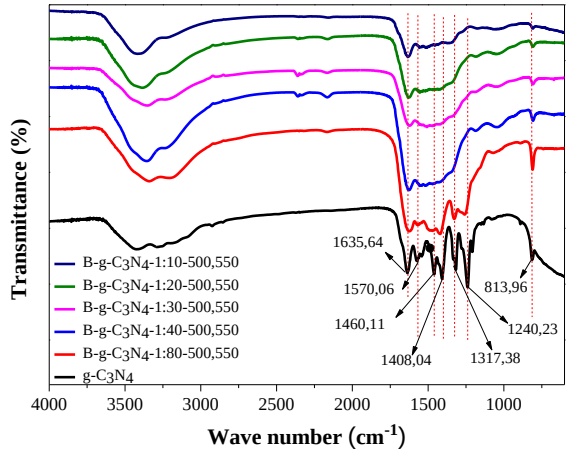

Figure 2. FT-IR spectra of g-C_3N_4 and B-g-C_3N_4-n:m-500,550.

Changes in the crystal structure of g-C_3N_4 with added boron were also investigated by FT-IR analysis. The results displayed in Figure 2 indicate that all doped samples still exhibit characteristic peaks of the structural bonds present in g-C_3N_4. This observation further confirms that boron doping does not alter the crystal structure of g-C_3N_4. Specifically, the peak at 813.96 cm^{-1} corresponds to the breathing mode of the tri-s-trazine units. Meanwhile, the range of peaks from 1240.23 to 1635.64 cm^{-1} is associated with the valence oscillation of C-N bonds in conjugated aromatic rings. Additionally, there are broad absorption bands in the range of 2900 to 3400 cm^{-1}, which correspond to the stretching vibration modes of the N-H bond and the hydroxyl group of adsorbed water molecules. Furthermore, it was observed that the intensity of the peaks in the range of 1240.23 to 1635.64 cm^{-1} slightly decreases with increasing boron content. This could be attributed to the overlap between the C-N stretch and the typical vibration of the B-N bond at 1370 cm^{-1}.[17,18]

3.2. Effect of the B concentration on the surface morphology of g-C_3N_4

The effect of the doped B content on the surface morphology of obtained samples was investigated by SEM. Figure 3 displays SEM images of both undoped g-C_3N_4 and boron-doped g-C_3N_4 samples with different resolutions.

Analysis of the SEM images shown in Figure 3 reveals that the surface morphology of the samples after boron doping does not differ significantly from that of the undoped sample. Additionally, it is worth noting that the particle sizes of all the obtained samples are in the nanoscale range.

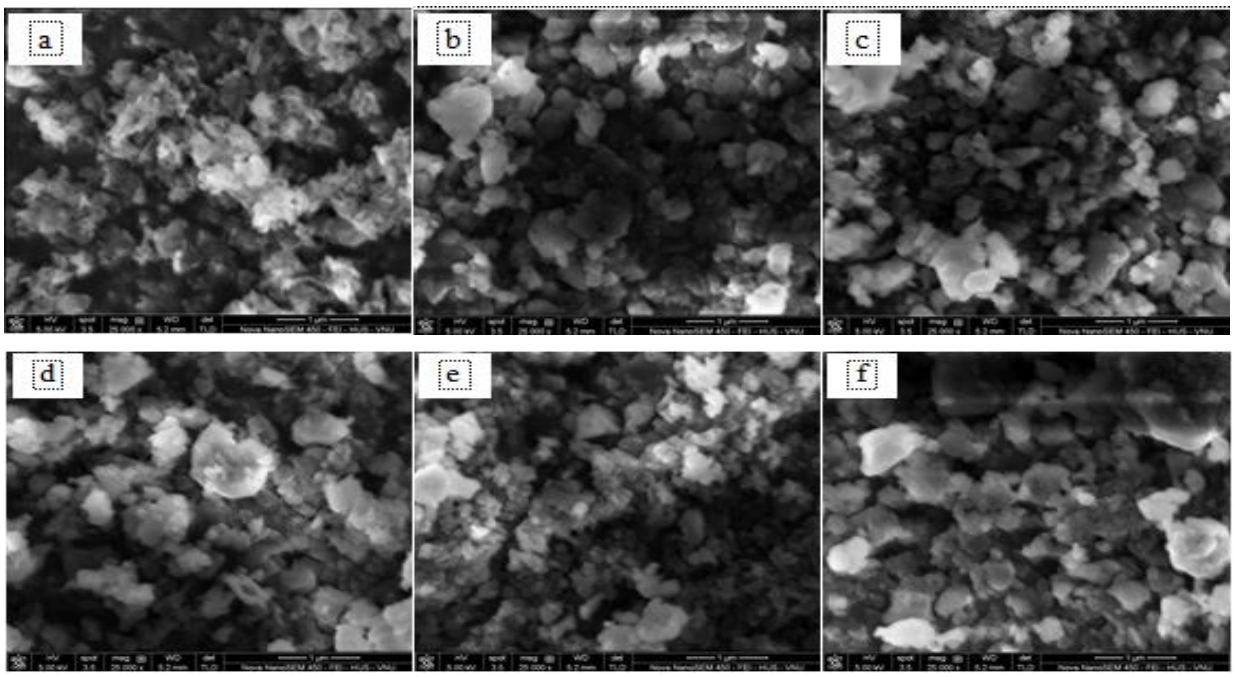

Figure 3. SEM images of g-C_3N_4 (a); B-g-C_3N_4-1:80 (b); B-g-C_3N_4-1:40 (c); B-g-C_3N_4-1:30 (d); B-g-C_3N_4-1:20 (e); B-g-C_3N_4-1:10 (f).

3.3. Effect of the B concentration on the band gap energy of g-C_3N_4

As the photocatalytic performance of semiconductors is strongly influenced by their optical absorption behavior, we used UV-Vis Diffuse Reflectance Spectroscopy (UV-Vis DRS) to investigate the optical absorption of g-C_3N_4 and B-g-C_3N_4-n:m samples. Figure 4 shows the UV-Vis DRS spectra of all the samples.

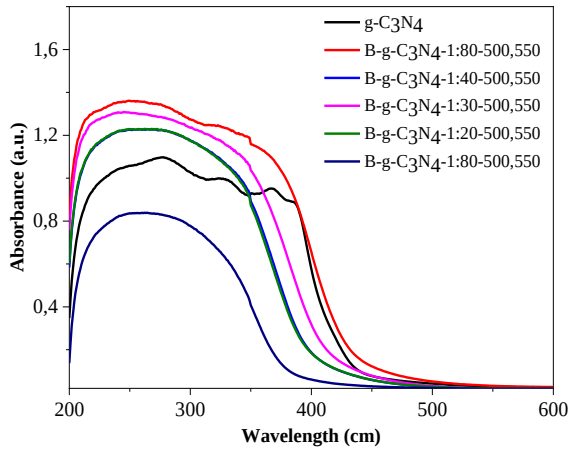

Figure 4. UV-Vis DRS spectra of g-C_3N_4 và B-g-C_3N_4-n:m samples.

Our findings reveal that most of the synthetic samples are capable of absorbing light in the visible region. The absorption band extends from the near-ultraviolet to the visible region, with the absorption edge occurring at a wavelength of approximately 500 nm. Compared to the g-C_3N_4 sample, the ability of most B-doped C_3N_4 samples to absorb light in the visible region slightly decreases. Notably, the B-g-C_3N_4-1:80 sample exhibits a stronger shift of the absorption edge towards longer wavelengths than the pure g-C_3N_4 sample and the remaining doped samples. This suggests that the B-g-C_3N_4-1:80 sample has the best adsorption capability in the visible region. The variation in absorption edges among the B-doped samples implies that B has become incorporated into the structure of g-C_3N_4, thereby altering the intrinsic electronic properties of pure g-C_3N_4.

To determine the band gap energy of the samples, we plotted a graph of Kubelka-Munk $[F(R)\ hv]^{1/2}$ dependence on absorbed photon energy. The results are presented in Table 1. It is worth noting that previous studies have demonstrated that boron doping in g-C_3N_4 leads to a reduction in the band gap energy.[14,18,19] However, in this particular study, the band gap (Eg) of the doped samples is generally higher than that of undoped g-C_3N_4 (which is 2.90 eV). This discrepancy may be attributed to the use of urea as the precursor in this research, instead of melamine or thiourea commonly used in other studies. The band gap energy increases with the B concentration, which suggests a decrease in the photocatalytic activities of boron-doped samples compared to undoped g-C_3N_4.

Table 1. Variation in the band gap energy for g-C_3N_4 and B-g-C_3N_4-n:m.

Sample	Band gap energy (eV)
g-C_3N_4	2.90
B-g-C_3N_4-1:80	2.86
B-g-C_3N_4-1:40	3.05
B-g-C_3N_4-1:30	2.97
B-g-C_3N_4-1:20	3.06
B-g-C_3N_4-1:10	3.22

3.4. Effect of the B concentration on photocatalytic activities of g-C_3N_4

The organic pollutant chosen to evaluate the photocatalytic performance of all the obtained samples was MB. Figure 5 shows the graph depicting the dependence of C/C_0 on time, where C_0 represents the concentration of the MB solution after 2 hours of being kept in the dark, and C represents the concentration of the MB solution after t (in hours) of irradiation.

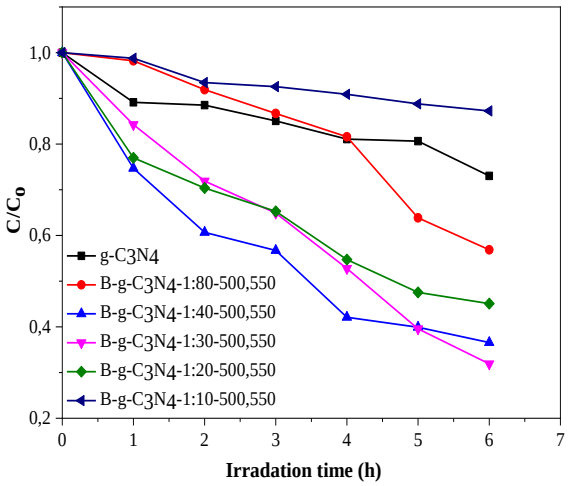

Figure 5. C/C_0 as a function of irradiation time for g-C_3N_4 và B-g-C_3N_4-n:m samples.

Figure 5 and Table 2 present the graph

and data, respectively, for the dependence of MB's C/C_0 on irradiation time and the photodegradation efficiency of boron-doped g-C_3N_4 and undoped g-C_3N_4 materials after 6 hours of irradiation. The experimental results demonstrate that the photodegradation efficiency increases with a small amount of B doping. Specifically, after 6 hours of irradiation, the catalytic efficiency of g-C_3N_4 is 26.97%, while B-g-C_3N_4-1:80-500,550 exhibits a higher efficiency of 43.13%. This improvement can be attributed to the decrease in the band gap energy of the pure material sample g-C_3N_4 (2.90 eV) compared to B-g-C_3N_4-1:80-500,550 (2.86 eV).

Table 2. MB photodegradation efficiency for g-C_3N_4 and B-g-C_3N_4-n:m samples after 6 hours of irradiation.

Sample	Photodegradation efficiency (%)
g-C_3N_4	26.97
B-g-C_3N_4-1:80	43.13
B-g-C_3N_4-1:40	63.44
B-g-C_3N_4-1:30	68.09
B-g-C_3N_4-1:20	54.90
B-g-C_3N_4-1:10	12.76

It is worth noting that the MB photodegradation efficiency of B-g-C_3N_4-1:10-500,550 is extremely low, at only 12.76%. This aligns well with the high band gap energy value of 3.22 eV, which prevents the photocatalyst from effectively absorbing visible light.

Compared to the g-C_3N_4 sample, B-g-C_3N_4-1:40, B-g-C_3N_4-1:30, B-g-C_3N_4-1:20, and B-g-C_3N_4-1:80 exhibit better catalytic decomposition performance. Notably, B-g-C_3N_4-1:30 showcases the highest photodegradation efficiency of 68.09%, making it the best material among the synthesized samples in terms of photocatalytic activity.

3.5. Evaluation of photocatalytic reaction kinetics

The kinetics of photocatalytic reactions for g-C_3N_4 and B-g-C_3N_4-n:m samples were evaluated using the Langmuir-Hinshelwood model, which represents the irradiation time dependence of the $\ln(C_0/C)$.

Figure 6 shows that the irradiation time dependence of $\ln(C_0/C)$ is linear. This indicates that the photodegradation of MB for both g-C_3N_4 and B-g-C_3N_4-n:m samples follows the Langmuir-Hinshelwood model, with a high coefficient of determination ($R^2 \geq 0.983$).

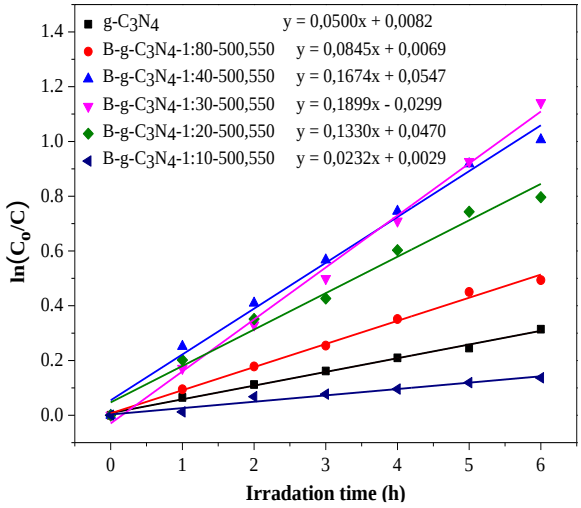

Figure 6. $\ln(C_0/C)$ as a function of irradiation time for g-C_3N_4 và B-g-C_3N_4-n:m samples.

The evaluation of the photocatalytic reaction kinetics, as shown in Table 3, reveals the obtained data for g-C_3N_4 and B-g-C_3N_4-n:m samples. It is observed that most of the boron-doped g-C_3N_4 samples have higher constant rates compared to the pure g-C_3N_4 sample. Specifically, the sample B-g-C_3N_4-1:30 exhibits the highest rate constant ($k = 0.1899$, $R^2 = 0.9955$), which is three times higher than the pure g-C_3N_4 sample ($k = 0.0500$, $R^2 = 0.9951$). This finding is consistent with their respective photocatalytic performances.

Table 3. Obtained data for g-C_3N_4 and B-g-C_3N_4-n:m samples as evaluation of photocatalytic reaction kinetics following the Langmuir – Hinshelwood model.

Sample	k_{app} (h^{-1})	R^2
g-C_3N_4	0,0500	0,9951
B-g-C_3N_4-1:80	0.0845	0.9951
B-g-C_3N_4-1:40	0.1074	0.9895
B-g-C_3N_4-1:30	0.1899	0.9955
B-g-C_3N_4-1:20	0.1330	0.9832
B-g-C_3N_4-1:10	0.0232	0.9623

3.6. Effect of the amount of catalyst on methylene blue photodegradation efficiency

The amount of photocatalyst plays a crucial role in heterogeneous photocatalysis as it directly affects the photocatalytic activities. In this study, we investigated the impact of varying photocatalyst amounts (0.01, 0.02, 0.03, 0.04, and 0.05 g) of B-g-C_3N_4-1:30-500,550 on the photocatalytic degradation of a 20 mg/L concentration of MB. The results are presented in Figure 7 and Figure 8.

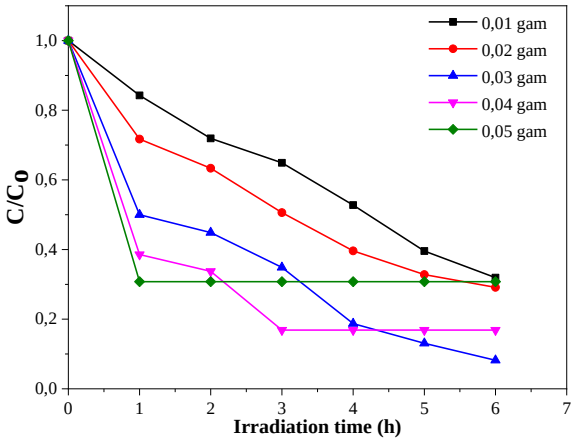

Figure 7. C/C_o as a function of the irradiation time with different amounts of B-g-C_3N_4-1:30.

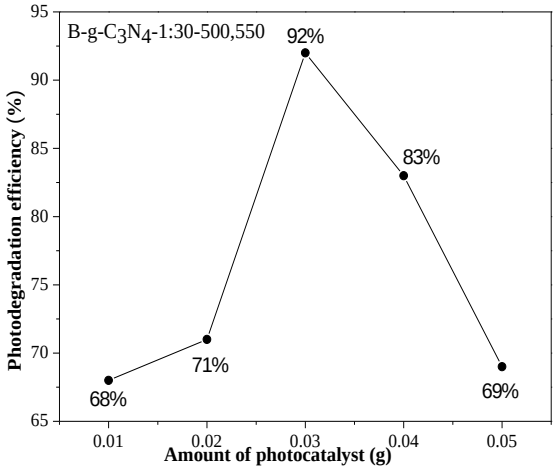

Figure 8. Photodegradation efficiency as a function of the photocatalyst amount for B-g-C_3N_4-1:30 after 6 hours of irradiation.

Figure 7 and Figure 8 illustrate that the photodegradation efficiency significantly increases from 68% to 92% as the amount of photocatalyst increases from 0.01 g to 0.03 g. This can be attributed to the larger number of active sites provided by the increased amount of photocatalyst, resulting in more free radicals HO• (the main agents involved in the decomposition of organic compounds). However, when the amount of photocatalyst exceeds 0.03 g and reaches 0.05 g, the photodegradation efficiency decreases from 92% to 69%. This decrease may be due to the increased turbidity of the solution resulting from a large amount of photocatalyst, which reduces its light absorption capacity and consequently diminishes the MB photodegradation efficiency.[20] Additionally, an excessive amount of photocatalyst can cause the agglomeration of catalyst particles, leading to a decrease in surface area and, consequently, a decrease in photodegradation efficiency.

4. CONCLUSION

This study focused on the synthesis and characterization of undoped g-C_3N_4 and boron-doped g-C_3N_4 photocatalysts. A simple condensation method was employed to synthesize the photocatalysts by heating urea alone or a mixture of urea and boric acid. Various techniques such as XRD, FT-IR, SEM and UV-Vis DRS were employed to investigate the effect of boron-doping on the crystal structure, surface morphology, bandgap energy, and photocatalytic properties of g-C_3N_4. The kinetics of photocatalytic reactions and the impact of the amount of photocatalyst on the efficiency of methylene blue (MB) photodegradation were examined. The results showed that all the samples exhibited photocatalytic activity in the visible light region. Particularly, the sample B-g-C_3N_4-1:30-500,550 exhibited the highest photodegradation efficiency of 92%.

REFERENCES

1. D. H. Kumar Reddy, S. M. Lee. Water Pollution and Treatment Technologies, *Journal of Environmental & Analytical Toxicology*, **2012,** *02*(05), e103.
2. S. Cao,J. Yu. g-C_3N_4-Based Photocatalysts for Hydrogen Generation, *Journal Phys Chem Lett*, **2014,** *5*(12), 2101−2107.
3. M. R. Gholipour, F. Béland,T.-O. Do. Graphitic Carbon Nitride-Titanium Dioxide Nanocomposite for Photocatalytic Hydrogen Production under Visible Light, *International Journal of Chemical Reactor Engineering*, **2016,** *14*(4), 851-858.
4. F. Dong, L. Wu, Y. Sun, M. Fu, Z. Wu,S. C. Lee. Efficient synthesis of polymeric g-C_3N_4 layered materials as novel efficient visible light driven photocatalysts, *Journal of Materials Chemistry*, **2011,** *21*(39).
5. G. Dong, Y. Zhang, Q. Pan,J. Qiu. A fantastic graphitic carbon nitride (g-C_3N_4) material: Electronic structure, photocatalytic and photoelectronic properties, *Journal of Photochemistry and Photobiology C: Photochemistry Reviews*, **2014,** *20*, 33-50.
6. X. Luo, Y. Dong, D. Wang, Y. Duan, K. Lei, L. Mao, Y. Li, Q. Zhao,Y. Sun. Facile synthesis of g-C3N4 nanosheets for effective degradation of organic pollutants via ball milling, *Reviews on Advanced*

Materials Science, **2023,** *62*(1), 20230123.
7. V. Vo, N. Van Kim, N. T. V. Nga, N. T. Trung, L. T. Giang, P. Van Hanh, L. H. Hoang,S.-J. Kim. Preparation of g-C_3N_4/Ta_2O_5 Composites with Enhanced Visible-Light Photocatalytic Activity, *Journal of Electronic Materials*, **2015,** *45*(5), 2334-2340.
8. Y. Kofuji, Y. Isobe, Y. Shiraishi, H. Sakamoto, S. Tanaka, S. Ichikawa,T. Hirai. Carbon Nitride-Aromatic Diimide-Graphene Nanohybrids: Metal-Free Photocatalysts for Solar-to-Hydrogen Peroxide Energy Conversion with 0.2% Efficiency, *J Am Chem Soc*, **2016,** *138*(31), 10019-10025.
9. M. Wu, J. M. Yan, X. N. Tang, M. Zhao,Q. Jiang. Synthesis of potassium-modified graphitic carbon nitride with high photocatalytic activity for hydrogen evolution, *ChemSusChem*, **2014,** *7*(9), 2654 – 2658.
10. M. Tahir, C. Cao, F. K. Butt, F. Idrees, N. Mahmood, Z. Ali, I. Aslam, M. Tanveer, M. Rizwan,T. Mahmood. Tubular graphitic-C_3N_4: a prospective material for energy storage and green photocatalysis, *Journal of Materials Chemistry A*, **2013,** *1*(44), 13949-13955.
11. Y. Hou, A. B. Laursen, J. Zhang, G. Zhang, Y. Zhu, X. Wang, S. Dahl,I. Chorkendorff. Layered nanojunctions for hydrogen-evolution catalysis, *Angew Chem Int Ed Engl*, **2013,** *52*(13), 3621-5.
12. L. Yang, X. Wang, J. Wang, G. Cui,D. Liu. Graphite carbon nitride/boron-doped graphene hybrid for efficient hydrogen generation reaction, *Nanotechnology*, **2018,** *29*(34), 345705.
13. S. Thaweesak, S. Wang, M. Lyu, M. Xiao, P. Peerakiatkhajohn,L. Wang. Boron-doped graphitic carbon nitride nanosheets for enhanced visible light photocatalytic water splitting, *Dalton Trans*, **2017,** *46*(32), 10714-10720.
14. S. C. Yan, Z. S. Li,Z. G. Zou. Photodegradation of rhodamine B and methyl orange over boron-doped g-C3N4 under visible light irradiation, *Langmuir*, **2010,** *26*(6), 3894–3901.
15. S. Tonda, S. Kumar, S. Kandula,V. Shanker. Fe-doped and -mediated graphitic carbon nitride nanosheets for enhanced photocatalytic performance under natural sunlight, *Journal of Materials Chemistry A*, **2014,** *2*(19), 6772–6780.
16. N. Sagara, S. Kamimura, T. Tsubota,T. Ohno. Photoelectrochemical CO_2 reduction by a p-type boron-doped g-C_3N_4 electrode under visible light, *Applied Catalysis B: Environmental*, **2016,** *192*, 193-198.
17. J. Wei, W. Shen, J. Zhao, C. Zhang, Y. Zhou,H. J. C. T. Liu. Boron doped g-C3N4 as an effective metal-free solid base catalyst in Knoevenagel condensation, **2018,** *316*, 199-205.
18. C. Lu, R. Chen, X. Wu, M. Fan, Y. Liu, Z. Le, S. Jiang,S. Song. Boron doped g-C3N4 with enhanced photocatalytic UO_2^{2+} reduction performance, *Applied Surface Science*, **2016,** *360*, 1016-1022.
19. P. Chen, P. Xing, Z. Chen, H. Lin,Y. He. Rapid and energy-efficient preparation of boron doped g-C3N4 with excellent performance in photocatalytic H2-evolution, *International Journal of Hydrogen Energy*, **2018,** *43*(43), 19984-19989.
20. H. M. Coleman, V. Vimonses, G. Leslie,R. Amal. Degradation of 1,4-dioxane in water using TiO_2 based photocatalytic and H2O2/UV processes, *J Hazard Mater*, **2007,** *146*(3), 496-501.